Journal of Colloid and Interface Science 590 (2021) 28–37

Contents lists available at ScienceDirect

Journal of Colloid and Interface Science

journal homepage: www.elsevier.com/locate/jcis

Regular Article

Co-immobilization of antioxidant enzymes on titania nanosheets for reduction of oxidative stress in colloid systems

Szilárd Sáringer [a], Paul Rouster [b], Istvan Szilagyi [a,*]

[a] MTA-SZTE Lendület Biocolloids Research Group, Interdisciplinary Excellence Center, Department of Physical Chemistry and Materials Science, University of Szeged, H-6720 Szeged, Hungary
[b] Institute of Condensed Matter and Nanosciences-Bio and Soft Matter, Université Catholique de Louvain, Louvain-la-Neuve B-1348, Belgium

GRAPHICAL ABSTRACT

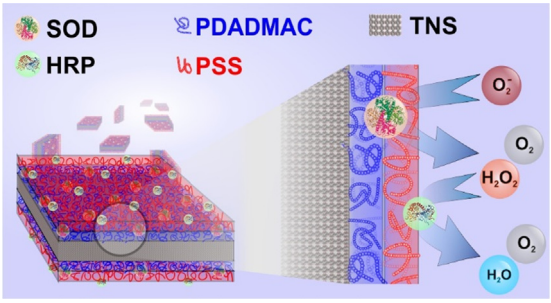

ARTICLE INFO

Article history:
Received 16 November 2020
Revised 4 January 2021
Accepted 5 January 2021
Available online 16 January 2021

Keywords:
Enzyme cascade
Immobilization
Titania nanosheets
Antioxidant composite
Sequential adsorption

ABSTRACT

Immobilization of single antioxidant enzyme systems was frequently studied in the past, however, there is a lack of reliable reports on the co-immobilization of such enzymes. Here, an antioxidant enzyme cascade involving superoxide dismutase (SOD) and horseradish peroxidase (HRP) was successfully immobilized on titania nanosheets (TNS) by the sequential adsorption method using poly (diallyldimethylammonium chloride) (PDADMAC) and poly(styrene sulfonate) (PSS) polyelectrolyte building blocks. The development of the cascade system was based on a colloid approach, in which the charging and aggregation processes were optimized in each synthetic step. The polyelectrolyte and enzyme multilayers were built up in two different sequences at the particle interface, namely, TNS-PDADMAC-SOD-PSS-HRP and TNS-HRP-PDADMAC-SOD-PSS. The formation of the polyelectrolyte layers led to charge reversal of the carrier and the saturated PDADMAC and PSS layers stabilized the dispersions, in particular, their resistance against salt-induced aggregation was especially excellent. The results of enzymatic assays revealed that the SOD and HRP-like activities of the composites depended on the location of the enzymes in the hybrid material. The obtained compounds showed remarkable antioxidant effect and were able to simultaneously decompose superoxide radical anions and hydrogen peroxide. The cascade systems are of great promise in industrial manufacturing processes during the preparation of high-quality products without any damages by reactive oxygen species.

1. Introduction

Normal biochemical reactions exposed to environmental effects and higher levels of dietary xenobiotics result in increased

* Corresponding author.
E-mail address: szistvan@chem.u-szeged.hu (I. Szilagyi).

https://doi.org/10.1016/j.jcis.2021.01.012
0021-9797/

generation of reactive oxygen species (ROS) such as superoxide (O_2^-), hydroxyl free radicals (OH^-) or hydrogen peroxide (H_2O_2) [1]. Extended ROS production induces oxidative stress leading to damage of cellular components such as DNA, proteins and lipids and also causes significant loss in the quality of industrial products [2–5]. The oxidative stress can be effectively neutralized by molecular and enzymatic antioxidants [6]. The latter ones, including superoxide dismutase (SOD) [7] and horseradish peroxidase (HRP) [8], are the most effective substances to combat oxidative stress, i.e., SOD dismutates O_2^- to molecular oxygen and H_2O_2, while HRP consumes H_2O_2 in oxidation reactions. They act together as an enzyme cascade in the cellular environments [9].

However, native enzymes are sensitive to the environmental conditions giving rise to limited stability, which impedes efficient delivery and supplementation of these proteins. The complex environment of the biological systems (e.g., high electrolyte concentration and presence of enzyme inhibitors) and the harsh environmental conditions (e.g., elevated temperature and pressure) in the industrial applications usually lead to enzyme denaturation and loss of enzymatic activity [10,11]. To overcome these limitations and broaden their applicability, considerable research activity was performed in the past decades to immobilize native enzymes in/on solid supports to improve their performances in organic solvents and their heat tolerances [12–14]. Furthermore, immobilization may enhance the structural stability and selectivity of the proteins providing long-term stabilization of the enzymes, which prevents dissociation-related inactivation [15]. Another advantage in the industrial applications is that the immobilized enzymes can be easily separated and removed from the reaction mixtures [16].

Concerning the antioxidant enzymes, immobilization of single proteins including SOD [17–19] and HRP [20–22] on various substrates was frequently reported in the past. However, co-immobilization of such enzymes could be an appropriate mimic of the cellular environment, where ROS are decomposed to molecular oxygen and water in tandem reactions catalyzed by the enzymes. To the best of our knowledge, only one system has been published, in which SOD and HRP were co-immobilized via covalent grafting to dendronized polymer chains [23,24]. Excellent antioxidant activity was achieved, however, the supporting polymer is hardly available and the grafting requires a complicated reaction. To achieve cost-effective and facile preparation of an immobilized antioxidant enzyme cascade, the solid support and the procedure have to be simplified.

Concerning the carrier, titania particles are promising candidates for the co-immobilization of SOD and HRP enzymes. Titania and its composites are versatile materials [25–28] and they are of great potential in enzyme immobilization owing to their advantageous surface properties as well as their chemical and thermal stability. Among them, titania nanosheets (TNS) possess well-defined layered or unilamellar structures associated with high surface area, good thermal stability, pH tunable properties and biocompatibility [29–31]. Although single antioxidant enzymes were immobilized on TNS structures using polyelectrolytes as stabilizing agents for instance [18–20,32,33], immobilized enzyme cascades were not reported so far. The use of polyelectrolytes allows the use of the sequential adsorption method [34] as a possible enzyme immobilization technique, which has already been applied on planar surfaces to embed proteins between polyelectrolyte layers [35–37]. However, there is a lack of studies dealing with the co-immobilization of enzymes on nanoparticulate supports applying the polyelectrolyte-based sequential adsorption technique.

The present study aims at the design of stable dispersions of nanoparticle-supported antioxidant enzyme cascade involving polyelectrolytes as building blocks. The co-immobilization of HRP and SOD was carried out by the sequential adsorption of oppositely charged polyelectrolytes (poly(diallyldimethylammonium chloride) (PDADMAC) and sodium poly(styrene sulfonate) (PSS)) on TNS particles through electrostatic forces. TNS was chosen as a solid support on the basis of our previous experiences in immobilization of single SOD [18] and HRP [20] enzymes, where it was observed that (i) the antioxidant activity remains similar upon enzyme adsorption on TNS, (ii) application of polyelectrolytes leads to improved colloidal stability and (iii) the obtained composites containing single enzymes possess all the advantages of a heterogeneous catalyst compared to the homogeneous counterpart. In addition, the use of catalase enzyme was also considered, but it lost its activity upon immobilization and hence, HRP was chosen as H_2O_2 consuming center in the hybrid material. Light scattering techniques were used to optimize the charging and aggregation features of the sub-systems during the preparation process to determine the conditions, under which the colloids are stable in order to obtain fine particle dispersions of high surface area. The enzymatic activity of the nanocomposites was determined in biochemical assays for different ROS substrates to assess the antioxidant activity.

2. Materials and method

2.1. Chemicals

Titania nanosheets (TNS) were synthetized by an established protocol detailed elsewhere [38]. Superoxide dismutase (SOD, from bovine liver), positively charged poly(diallyldimethylammonium chloride) (PDADMAC, 20 wt%, average molecular mass of 275 kg/mol), negatively charged poly(styrene sulfonate) (PSS, sodium salt, molecular mass of 10.6 kg/mol), xanthine oxidase (lyophilized powder, 0.4–1.0 units/mg protein) were purchased from Sigma-Aldrich (Budapest, Hungary). Horseradish peroxidase (HRP), NaCl, H_2O_2, NaH_2PO_4 (anhydrous) and Na_2HPO_4 (anhydrous) were purchased from VWR (Debrecen, Hungary). Xanthine (99%) was bought from Alfa Aesar (Karlsruhe, Germany). Nitro blue tetrazolium (NBT) chloride monohydrate and guaiacol (99%) were acquired from Acros (Debrecen, Hungary). Ultrapure water was produced with a VWR Puranity TU+ device for all the sample preparations. Salt solutions were filtered with a 0.1 μm PVDF syringe filter purchased from Millex (Budapest, Hungary). The measurements were carried out at pH 7 and 25 °C, unless stated otherwise. Prior to use, TNS were dispersed in ultrapure water. Samples containing PDADMAC and PSS in a concentration range of 0.001–100 mg/L were obtained by dissolving the polyelectrolytes in ultrapure water. SOD and HRP enzymes were dissolved in ultrapure water and solutions with a concentration range of 0.001–40 mg/L were prepared.

2.2. Electrophoretic mobility

Electrophoretic mobilities were determined by electrophoretic light scattering with a Litesizer 500 instrument (Anton Paar, Graz, Austria) equipped with a 40 mW semiconductor laser operating at 658 nm wavelength. For all the measurements, 1 mL solutions were prepared. Accordingly, 0.1 mL of the TNS dispersions of 10 mg/L concentration was added to 0.9 mL solution composed of the calculated amount of polyelectrolyte, enzyme and NaCl, the latter one is to set the ionic strength. The samples were allowed to rest 2 h at room temperature before measuring the electrophoretic mobilities after 1 min equilibration time in the device. The reported values are the average of five individual measurements. The experiments were performed in 350 μL volume omega-shaped plastic cuvettes (Anton Paar). The average error of the method is 5%.

2.3. Dynamic light scattering

To determine the hydrodynamic radius (R_h) of the particles, dynamic light scattering (DLS) experiments were carried out with the same Litesizer 500 instrument as used in the mobility study. The cumulant fit [39] was used to fit the correlation function, which was collected for 20 s at 175° scattering angle. Time-resolved DLS measurements were performed to determine the apparent aggregation rate coefficient (k_{app}) of particle dimer formation as [40]

$$k_{app} = \frac{1}{R_h(0)} \frac{dR_h(t)}{dt} \quad (1)$$

where t is the time of the experiment and $R_h(0)$ is the hydrodynamic radius of the TNS determined in a stable dispersion. Examples for time-resolved DLS measurements are shown for the different systems in the Supplementary material in Fig. S1a–d.

The measurements were run for 40–120 min depending on the speed of aggregation. The same particle concentration (1 mg/L) was used in all of the time-resolved measurements. To compare the tendencies, the sample preparation for the DLS was done in a similar manner as the one described above for electrophoresis. The only difference was that the total volume was 2 mL for DLS and that the measurements were started directly after adding the particles to the solutions of polyelectrolyte, enzyme and NaCl. The samples were stirred with a Vortex before starting the time-resolved experiments. The colloidal stability was expressed in terms of stability ratio (W), which was calculated from the k_{app} values as follows [18,40,41]

$$W = \frac{k_{app}^{fast}}{k_{app}} \quad (2)$$

where the fast condition corresponds to the diffusion-controlled aggregation of the particles achieved in 1 M NaCl solution. One can realize that a stability ratio of unity is associated to unstable dispersions, where all the particle collisions result in dimer formation. Note that the above protocol leads to a mean error of 10%.

2.4. Transmission electron microscopy

The morphology of the materials was explored by transmission electron microscopy (TEM). The TEM images were recorded on a Tecnai G2 Sphera microscope (FEI, Hillsboro, USA) at an acceleration voltage of 120 kV using a LaB6 cathode. The samples were prepared by placing 5 μL of solution on a plasma-treated carbon mesh and by removing the excess liquid after 2 min. The obtained mesh with the material was installed on the sample holder and placed in the electron microscope. The drying process induced the formation of some particle aggregates.

2.5. Enzymatic assays

To determine the SOD-like activity of the obtained materials, the Fridovich method was employed [42]. However, the enzymatic assay protocol had to be slightly modified to adapt to the high scattering from the suspended TNS. Each sample was composed of xanthine (3 mM, 0.1 mL), NBT (3 mM, 0.1 mL), xanthine oxidase (3 mg/mL, 0.3 mL) and dispersion containing the catalyst (bare or immobilized SOD, 0–2.5 mL) in phosphate buffer and completed to a final volume of 3 mL. The phosphate buffer concentration in the samples was 2.7 mM and the pH was set at 7. Once all the reagents were mixed, the increase in the absorbance band at 565 nm was monitored for 6 min. The increase in the absorbance (ΔA_s) was determined for several SOD concentrations. Due to the scattering of the TNS particles, the corresponding samples without SOD were used as references (ΔA_0). The inhibition (I) of the superoxide radical anion (O_2^-)-NBT reaction was then calculated as

$$I = \frac{\Delta A_0 - \Delta A_s}{\Delta A_0} \cdot 100 \quad (3)$$

The O_2^- scavenging activities were expressed as IC_{50} values, which correspond to the SOD concentration needed to dismutate 50% of the O_2^- formed in the probe reaction.

The determination of the HRP activity was performed using the guaiacol assay [19,43,44]. In brief, 240 μL of the bare or immobilized HRP sample containing 10 mg/L enzyme was mixed with 240 μL of phosphate buffer (100 mM) followed by the addition of appropriate amount of guaiacol solution of 100 mM concentration and completed to a volume of 1680 μL with ultrapure water. Finally, 720 μL of H_2O_2 (9 mM) was added into the cuvette, which was vortexed again and immediately introduced into the UV–vis spectrophotometer to follow the formation of the guaiacol degradation products at 470 nm wavelength [45]. The increase in the absorbance was monitored as a function of the reaction time and the linear part of the curve was fitted to calculate the reaction rate (v). The Michaelis constant (K_m) and the maximum reaction rate (v_{max}) were calculated by the Lineweaver-Burk equation as follows [46]

$$\frac{1}{v} = \frac{K_m}{v_{max}} \frac{1}{[S]} + \frac{1}{v_{max}} \quad (4)$$

where $[S]$ refers to the guaiacol concentration.

3. Results and discussion

The development of the enzyme cascade by the sequential adsorption technique requires stable dispersions of functionalized TNS in each steps of the process. Therefore, the colloidal stability of the sub-systems was optimized by investigating the surface charge and aggregation of the particles at different concentrations of the polyelectrolytes and enzymes. The resistance against salt-induced aggregation of the obtained cascade was also studied to assess the colloidal stability. Finally, the antioxidant activity was measured in dismutation of O_2^- and in the consumption of H_2O_2. Note that the immobilization of single SOD [18] and HRP [20] on TNS has been reported earlier, while the present study focuses on their co-immobilization.

3.1. Build-up of PDADMAC/PSS bilayer on TNS

Given the negative surface charge of TNS under the conditions investigated [38], the effect of the oppositely charged PDADMAC on the charging and aggregation of bare TNS was first studied by electrophoresis and DLS. The electrophoretic mobilities recorded at different PDADMAC loadings are presented in Fig. 1.

Strong adsorption of PDADMAC on oppositely charged surfaces was reported in the past [38,47–49], which was also observed in the present system. The adsorption process was clearly indicated by the progressive increase in the mobility values by increasing the PDADMAC concentration. Such an adsorption led to charge neutralization at the isoelectric point (IEP). Furthermore, the adsorption process continued after the charge neutralization point and charge reversal of the TNS particles occurred. Such an inversion of the original charge is typical for colloidal particles in the presence of oppositely charged polyelectrolytes [38,47,49–53]. At high doses, the surface became saturated with the adsorbed PDADMAC and hence, the electrophoretic mobilities reached a plateau at 150 mg/g. Note that the onset of this plateau is given by the intersection of the linear fits applied on the mobility data of the increasing region and of the plateau. For the latter one, a zero slope was

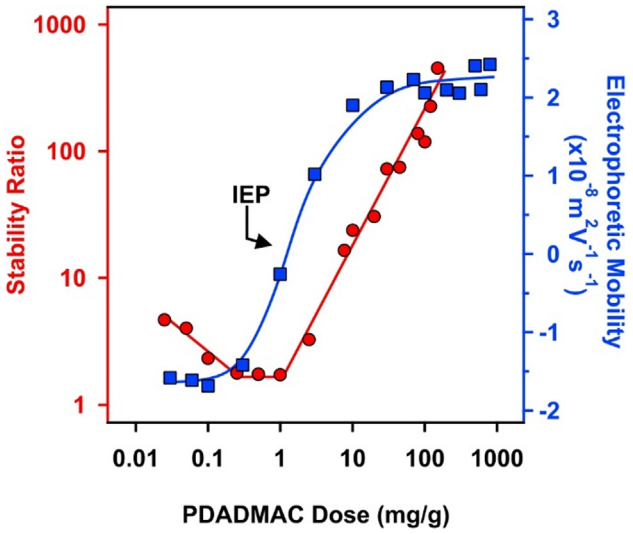

Fig. 1. Stability ratio (red circle) and electrophoretic mobility (blue square) of the TNS versus the PDADMAC dose. The ionic strength and the TNS concentration were 1 mM and 1 mg/L, respectively. The unit in the x-axis indicates mg of PDADMAC per 1 g of TNS. The lines serve to guide the eyes. The average error of the stability ratio and the mobility values are 10 and 5% respectively. (For interpretation of the references to colour in this figure legend, the reader is referred to the web version of this article.)

applied. One can notice that the charge reversal gave rise to a higher magnitude of charge, when comparing the mobilities measured at the lowest and highest PDADMAC doses.

DLS represents an excellent tool to determine the size of the colloidal particles in dispersions [41,54] and subsequently, to measure the rate of particle aggregation processes [40,41,52]. Therefore, stability ratio values were calculated from the rate constants determined at different PDADMAC doses in time-resolved DLS experiments (Fig. 1). The stability ratios close to unity indicated unstable dispersions at the IEP, while they steeply increased beyond the IEP giving rise to stable dispersions at high doses, after the adsorption saturation point discussed in the mobility studies. At low doses, however, a limited stability and low stability ratios were obtained.

The aggregation features of TNS at different PDADMAC doses resembles to the one predicted by the classical theory developed by Derjaguin, Landau, Verwey, and Overbeek (DLVO) [55]. Indeed, the nanosheets rapidly aggregate once the surface charges are neutralized at the IEP, where the repulsive electrical double layer interaction is absent and the attractive van der Waals force predominates. When the nanosheets possessed sufficient charge at high doses, the repulsive electrical double-layer forces stabilized the samples in conjunction with the DLVO theory. On the other hand at low polyelectrolyte doses, limited stability was achieved, which originates from the low charge of the bare particles and to the additional non-DLVO attractive forces, which is related to the so called patch charge effect due to polyelectrolyte adsorption at lower surface coverage [38,49,50].

Based on these results, a PDADMAC dose of 150 mg/g (denoted as TNS-PDADMAC in the following) was selected for the further steps of the sequential adsorption process. Under this condition, PDADMAC formed a saturated layer on the surface of the TNS giving rise to a stable dispersion of positively charged particles. In addition, the obtained TNS-PDADMAC possess higher colloidal stability than the bare particles. The net positive surface charge allows the immobilization of the negatively charged SOD enzyme through electrostatic interactions.

In the next step, the conditions were optimized to build-up a PSS layer on the TNS-PDADMAC. A major requirement was to achieve high colloidal stability after the bilayer formation on the TNS particles. Accordingly, negatively charged PSS was adsorbed on the TNS-PDADMAC hybrid. Although, the PDADMAC/PSS multilayer formation was frequently reported on planar substrates [56–58], very limited information is available with nanoparticles acting as carrier for the multilayer [59]. Electrophoretic mobilities were first determined to probe the influence of the PSS concentration on the charging behavior of the TNS-PDADMAC (Fig. 2).

Considering the change in the magnitude of the electrophoretic mobilities, very similar tendencies were observed as in the systems containing only TNS and PDADMAC. PSS adsorption was clearly indicated by the decrease of the mobilities by increasing the PSS concentration. Such an adsorption process led to charge neutralization at the IEP and charge reversal at higher doses. The adsorption continued until the mobilities reached a plateau at 300 mg/g.

Stability ratio measurements revealed that the particles were stable at low and high polyelectrolyte doses. In the intermediate regime, the stability ratios formed a V-shape curve with a minimum near the IEP. This behavior is again in line with the DLVO theory, i.e., the acting interparticle forces are of electrostatic origin [55]. A major difference from the above system is that, the fast aggregation regime is extremely narrow. These results ensure that at 300 mg/g dose the TNS-PDADMAC-PSS particles are negatively charged and form highly stable colloids.

Note that the minimum of the stability ratio values was around 3 instead of 1 (the prediction of the DLVO theory), which indicates the presence of additional stabilizing forces. Since the fast aggregation rate of the TNS was used to calculate the stability ratios by equation (2), such a stabilizing effect must originate from the adsorbed polyelectrolyte layers. It was assumed that repulsive steric interactions are responsible for this phenomenon, however, this assumption deserves further discussion.

Accordingly, around the IEP, the overall charge of the particles is close to zero, which leads to a limited stability of the particles due to the absence of the electrostatic double layers and the sole presence of attractive van der Waals forces. Under these conditions, DLVO theory states that each particle collision must result in the formation of a dimer and the stability ratio values must be around unity in case of diffusion-controlled aggregation. However, when PSS is adsorbed on the PDADMAC layer of the particles, intrinsic

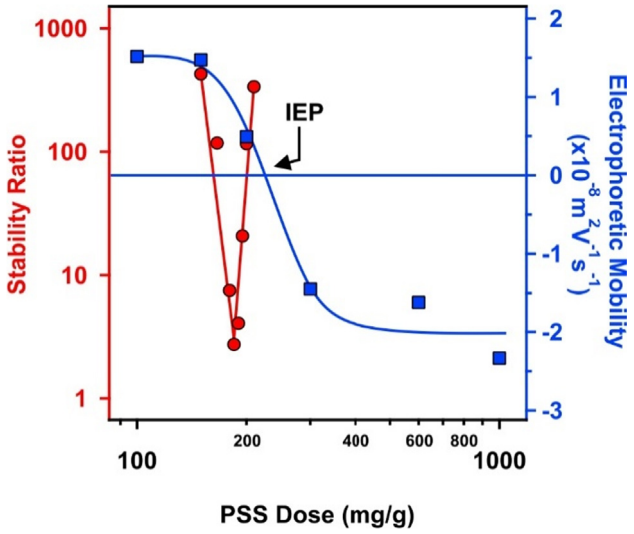

Fig. 2. Stability ratio (red circle) and electrophoretic mobility (blue square) of the TNS-PDADMAC as a function of the PSS dose at 1 mg/L TNS concentration and 1 mM ionic strength. The average error of the stability ratio and the mobility values are 10 and 5% respectively. (For interpretation of the references to colour in this figure legend, the reader is referred to the web version of this article.)

polymer-polymer and extrinsic polymer-ion charge compensations occur [60]. The ion compensated PSS charges on the polymer backbone form tails and loops dangling in the solution [61], which leads to the generation of a steric repulsion between the particles due to the raising osmotic pressure upon approach of the polyelectrolyte coated surfaces [62]. This effect, together with the electrostatic stabilization by the double layers leads to electrosteric stabilization [54], which was reported in various particle-polyelectrolyte systems [38,52,59]. Nevertheless, such an electrosteric repulsion is not sufficient to completely prevent particle aggregation here, as the stability ratio value is around 3 at the minimum.

3.2. Co-immobilization of the enzymes

The SOD and the HRP enzymes are negatively and positively charged at pH 7, since their pI values are 4.95 [63] and 8.80 [64], respectively. Therefore these enzymes are expected to adsorb on oppositely charged particles mainly by electrostatic attraction [18,20]. However, hydrophobic interactions and hydrogen bonding may play a role in the adsorption mechanism too. It was unambiguously confirmed before that positively charged TNS-PDADMAC forms highly stable colloids and hence, it is a suitable support for SOD. Moreover, extensive SOD adsorption may affect the charging and aggregation properties of TNS-PDADMAC. In other words, it is important to avoid a significant decrease in the magnitude of the surface charge upon enzyme adsorption because it may lead to a weakening of the double layer repulsion and subsequently, to unwanted particle aggregation. Therefore, the influence of SOD adsorption on the electrophoretic mobilities was first probed by recording the mobilities at different SOD concentrations (Fig. 3).

The results revealed that for an enzyme dose lower than 100 mg/g the mobility values of TNS-PDADMAC were not affected by the added amount of SOD. Above this loading, the magnitude of the mobilities slightly decreased. Note that no stability ratio values could be determined in the SOD concentration range investigated due to the high stability, i.e., the lack of aggregation processes, of the colloidal dispersion. Therefore, a SOD dose of 10 mg/g was selected for the further steps. Earlier studies on a slightly different system [18] revealed that at this concentration the enzyme was quantitatively adsorbed and does not desorb from the particle surface. The obtained TNS-PDADMAC-SOD material (150 mg/g PDADMAC and 10 mg/g SOD) was then used to build up the PSS layer applying a 300 mg/g PSS loading (denoted as TNS-PDADMAC-SOD-PSS later), as discussed in the previous section.

The same requirements apply for the HRP adsorption on TNS-PDADMAC-SOD-PSS, therefore, the electrophoretic mobilities were measured at different enzyme loadings (Fig. 3). As a matter of fact, it is primordial to determine an HRP dose, which does not affect the colloidal behavior of the TNS. The mobility values were not changed significantly and no stability ratios could be determined in the enzyme dose regime studied. Based on the results of an earlier study [20], 10 mg/g concentration was selected for the HRP. At this dose, HRP adsorption does not significantly alter the charging and aggregation behavior of TNS-PDADMAC-SOD-PSS, and on the other hand, quantitative enzyme adsorption is expected. Accordingly, 10 mg/g dose was applied for both SOD and HRP embedded in the TNS-PDADMAC-SOD-PSS-HRP composite.

An overview of the electrophoretic mobilities and the hydrodynamic size of the sub-systems during the sequential adsorption process is shown in Fig. 4. The electrophoretic mobility of the bare particles is around -1.5×10^{-8} m^2/Vs. This slight negative charge led to a moderate stability and to higher hydrodynamic radius value due to the presence of particle aggregates. Nevertheless, the formation of the saturated PDADMAC layer provided an improved stability and thus, the radius of the positively charged TNS-PDADMAC decreased from 145 nm (bare TNS) to about 100 nm. The immobilization of SOD at 10 mg/g did not change the mobility significantly and slightly decreased the size. After the functionalization with the saturated PSS layer, the TNS-PDADMAC-SOD-PSS system possesses a negative charge with a mobility about -1.9×10^{-8} m^2/Vs. Note that very similar value for the TNS led to limited stability and formation of particle aggregates. However, the radius of TNS-PDADMAC-SOD-PSS was much lower compared to bare TNS. This result again sheds light on the

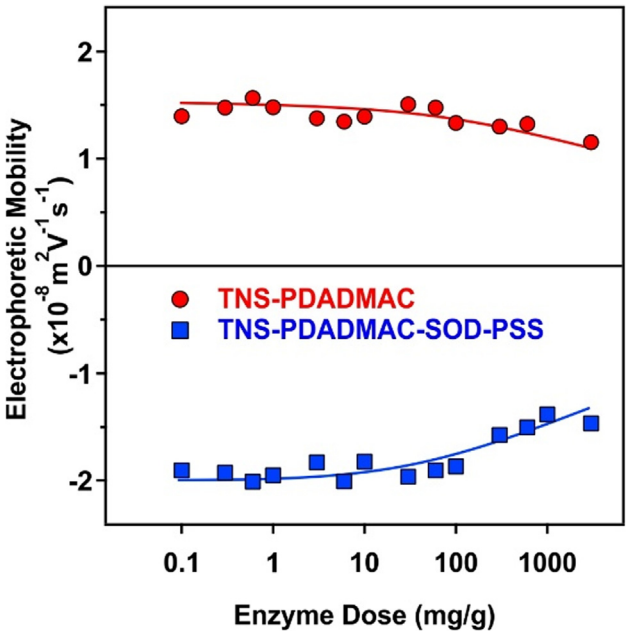

Fig. 3. Electrophoretic mobility of the TNS-PDADMAC (red circles) and the TNS-PDADMAC-SOD-PSS (blue squares) hybrid materials as a function of the enzyme (SOD and HRP, respectively) dose at pH 7, 1 mM ionic strength and 1 mg/L TNS concentration. The average error of the mobility values is 5%. (For interpretation of the references to colour in this figure legend, the reader is referred to the web version of this article.)

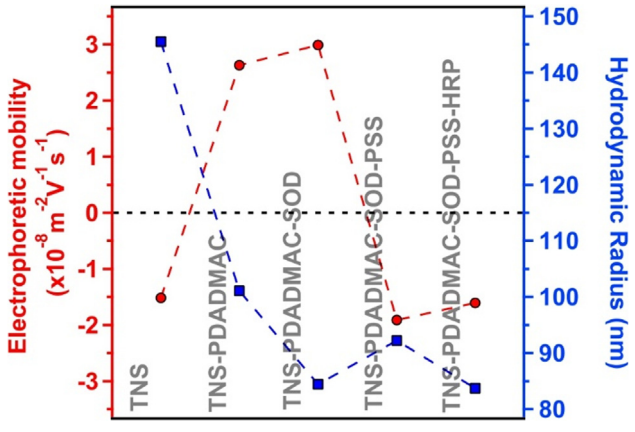

Fig. 4. Electrophoretic mobility (red circle) and hydrodynamic radius (blue square) at different steps during the sequential adsorption process. The ionic strength and the TNS concentration were set to 1 mM and 1 mg/L, respectively. The used PDADMAC and PSS doses were 150 and 300 mg/g, respectively, while 10 mg/g loadings were applied for both SOD and HRP enzymes. The connective dashed lines are to guide the eyes and the horizontal one indicates the zero electrophoretic mobility. The measurement error for both size and mobility is 5%. (For interpretation of the references to colour in this figure legend, the reader is referred to the web version of this article.)

importance of steric forces (see in the previous chapter) in the stabilization mechanism, since sole electrostatic repulsion fails to stabilize the colloids at this low mobility. The surface charge and hydrodynamic size did not change upon HRP immobilization in the last step of the sequential adsorption procedure.

TEM images recorded with the TNS-PDADMAC-SOD-PSS-HRP (Fig. 5) show the rectangular shape of the TNS. The morphology of the particles remained unaffected during the layer formations indicated by very similar images compared to the ones of the bare TNS without surface functionalization [38]. However, some low order aggregates of the particles can be observed. This is due to the drying of the samples, which could not be avoided during the TEM measurements.

3.3. Salt-induced aggregation

Given the fact that immobilized enzymes are often used in liquid environments containing electrolytes [16], the resistance of the fabricated hybrid material against salt-induced aggregation was tested. Accordingly, the ionic strength was systematically changed in the dispersions of the bare TNS and the TNS-PDADMAC-SOD-PSS-HRP material. Electrophoretic mobilities and stability ratios are presented in Fig. 6.

At low ionic strength, the mobility values of the bare TNS and the TNS-PDADMAC-SOD-PSS-HRP were about -1.5×10^{-8} m^2/Vs and -2.4×10^{-8} m^2/Vs, respectively (Fig. 6a). This difference indicates the development of higher surface charge upon multilayer formation. By increasing the ionic strength, the mobilities increased in both systems owing to the screening effect of the dissolved salt constituents on the surface charges.

The aggregation behavior at different ionic strengths were investigated by time-resolved DLS technique and the obtained stability ratios are shown in Fig. 6b. The slow and fast aggregation regimes, separated by the critical coagulation concentration (CCC) values, were observed in each case. The stability of the TNS was very limited even at low ionic strengths due to the low charge of the particles. The difference in the CCC values is striking, 10 and 300 mM were determined for TNS and TNS-PDADMAC-SOD-PSS-HRP, respectively. The stabilizing effect is twofold. On the one hand, higher surface charge indicated by higher magnitude of the mobilities led to stronger repulsion by the overlapping electrical double layers, in line with the DLVO theory. However, DLVO usually predicts CCC values around 100 mM and thus, additional repulsive forces are most likely present in the composite system. Similar to the TNS-polyelectrolyte sub-systems, this repulsion originates from steric interactions [52,54,59,62] between the loosely adsorbed polyelectrolyte chains extending towards the solution phase from the multilayered structure. The overlap of polyelectrolyte tails and loops lead to the raise of an osmotic pressure upon the approach of two particles and subsequently, to the development of repulsive interparticle forces.

3.4. Enzymatic activity

The O_2^- scavenging activities of the native and immobilized SOD enzyme were tested in the Fridovich assay [42], as detailed in the experimental part. The inhibition versus enzyme concentration graph (Fig. 7a) indicates a maximum inhibition of about 65% for TNS-PDADMAC-SOD-PSS-HRP material indicating a limited accessibility towards O_2^- for the immobilized SOD.

An IC_{50} value of 1.3 mg/L was obtained, which is significantly higher than the one determined for the TNS-PDADMAC-SOD subsystem (Table 1). Note that the higher IC_{50} value means lower SOD activity and that the TNS-PDADMAC-PSS-HRP did not show any SOD-like activity in this concentration range. These data indicate that the building of the PSS-HRP layers on the TNS-PDADMAC-SOD led to a significant loss in the SOD-like activity. This may be due to some conformational changes of the enzyme upon immobilization and/or to some blocking effects of the outer polyelectrolyte layer, i.e., the hindered diffusion of the O_2^- to the active site of the SOD.

The HRP-like activities were determined by the guaiacol assay [45]. Briefly, the HRP-active compound catalyzes the oxidation of the guaiacol substrate in the presence of H_2O_2 and the formation of the brownish guaiacol degradation products can be monitored with a spectrophotometer. No enzymatic activity was observed for materials without the HRP component (Table 1), so the enzyme-like function originated solely from this enzyme embedded in the composites.

The Lineweaver–Burk plot (see equation (4)) was used to analyze the results of the HRP assay and the Michaelis constant (K_m) together with the maximum reaction rate (v_{max}) were calculated from the double reciprocal reaction rate versus the substrate concentration plot as shown in (Fig. 7b). The K_m value corresponds to the affinity of the enzyme towards the substrate. For example, a decrease in the K_m value refers to a higher affinity of the enzyme to guaiacol. The v_{max} is the maximum reaction rate that can be achieved by the system once the active site of the enzymes is completely saturated by the substrate.

The determined K_m and v_{max} values for the TNS-PDADMAC-SOD-PSS-HRP were 23.50 mM and 0.10 mM/s, respectively. These data indicate a lower activity compared to the native enzyme, however, it can still be considered as a highly active material. A possible explanation may lie in the fact that HRP is located on the outer surface of the TNS-PDADMAC-SOD-PSS-HRP particles and thus, interacting strongly with PSS upon immobilization,

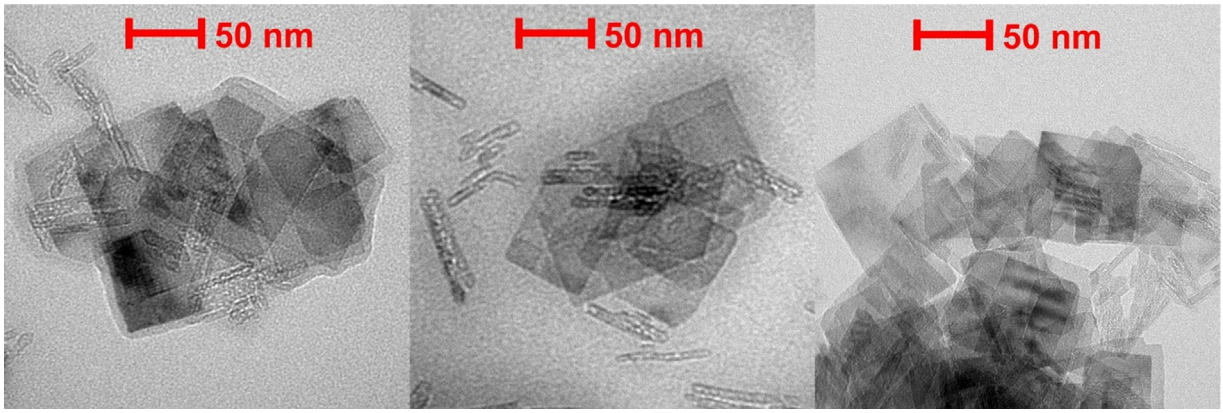

Fig. 5. Dried-stage TEM images of the TNS-PDADMAC-SOD-PSS-HRP cascade material.

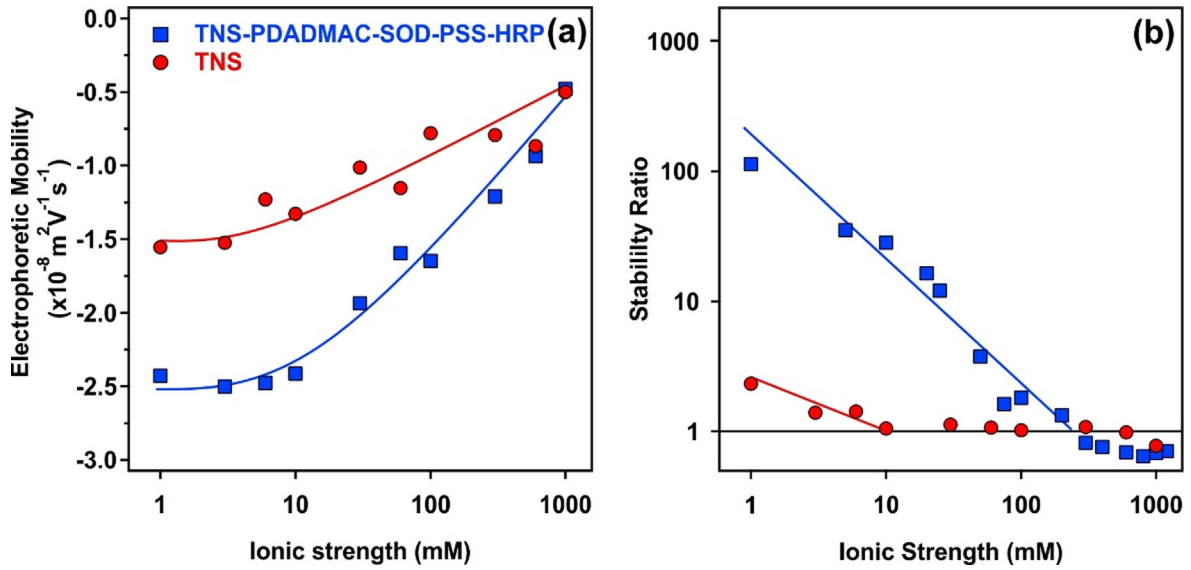

Fig. 6. Electrophoretic mobility (a) and stability ratio (b) of the bare TNS (red circles) and the TNS-PDADMAC-SOD-PSS-HRP (blue squares) hybrid material as a function of the ionic strength adjusted with NaCl. The TNS concentration was set to 1 mg/L. The lines serve to guide the eyes. The mean error of the stability ratio and the mobility values are 10 and 5% respectively. (For interpretation of the references to colour in this figure legend, the reader is referred to the web version of this article.)

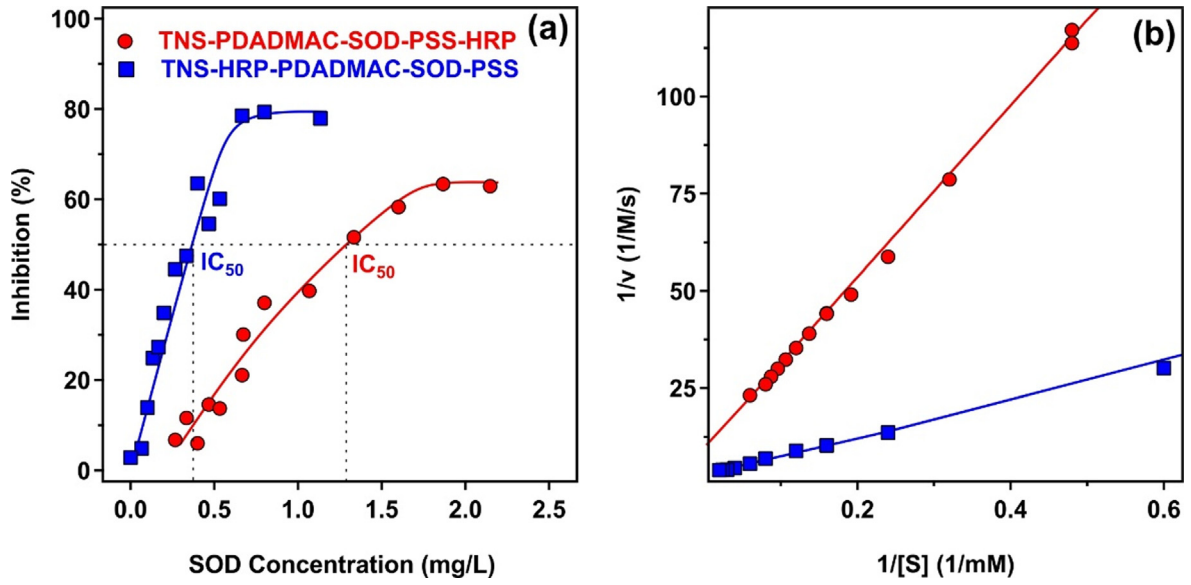

Fig. 7. (a) Inhibition of the NBT-O_2^- reaction by the TNS-PDADMAC-SOD-PSS-HRP (red circles) and the TNS-HRP-PDADMAC-SOD-PSS (blue squares) hybrid particles. The inhibition values were obtained using equation (3). The solid line is a mathematical function used for the interpolation of the IC_{50} value. (b) Lineweaver–Burk plot for the peroxidase activity of the TNS-PDADMAC-SOD-PSS-HRP and the TNS-HRP-PDADMAC-SOD-PSS hybrid particles. The solid line was obtained using equation (4). The average error of the measurements is within 5%. (For interpretation of the references to colour in this figure legend, the reader is referred to the web version of this article.)

Table 1
Parameters determined in the SOD and HRP assays.

Material	IC_{50} (mg/L)	Maximum inhibition (%)	K_m (mM)	v_{max} (mM/s)
SOD	0.10 ± 0.01	90 ± 5	N/A[a]	N/A[a]
HRP	N/A[a]	N/A[a]	3.41 ± 0.15	0.59 ± 0.02
TNS-PDADMAC-SOD	0.22 ± 0.01	70 ± 4	N/A[a]	N/A[a]
TNS-PDADMAC-SOD-PSS-HRP	1.30 ± 0.04	65 ± 4	23.50 ± 2.27	0.10 ± 0.01
TNS-HRP	N/A[a]	N/A[a]	13.13 ± 1.17	0.41 ± 0.02
TNS-HRP-PDADMAC-SOD	0.15 ± 0.01	90 ± 5	3.91 ± 0.64	0.31 ± 0.04
TNS-HRP-PDADMAC-SOD-PSS	0.38 ± 0.03	80 ± 4	15.50 ± 1.19	0.34 ± 0.01

[a] N/A means that no measurable activity was detected.

which may have led to a distortion of the structure of its active center giving rise to a lower activity of the developed system compared to the native enzyme dissolved in solution.

3.5. Variation of the TNS coating architecture in the sequential adsorption method

To probe the influence of the location of the enzymes on their activities, the order of the building blocks was changed during the preparation of the enzyme cascade. In an earlier study, HRP was immobilized directly on the TNS particles without the use of any intermediate polyelectrolyte layer [20]. Therefore the multilayered architecture was built on the TNS-HRP hybrid following the TNS-HRP-PDADMAC-SOD-PSS order. The same polyelectrolyte and enzyme doses were used as in the TNS-PDADMAC-SOD-PSS-HRP system and the obtained mobility and size data measured for the system at each building steps are displayed in Fig. 8. The changes in the electrophoretic mobilities and the particle sizes during the sequential adsorption steps clearly indicated that the immobilization of HRP did not significantly influence the charging behavior of the bare TNS particles (Fig. 8). However, addition of HRP somehow increased the size, i.e., about 400 nm hydrodynamic radius was determined for TNS-HRP. Like for the previous systems, adsorption of a saturated PDADMAC layer gave rise to charge reversal and to a significant decrease in the particle size due to electrosteric stabilization. The immobilized SOD had basically no effect on the colloidal stability of the dispersions, while the adsorption of the PSS layer resulted in charge reversal of the particles. It should be noted that the mobility values of TNS-HRP-PDADMAC-SOD-PSS was very similar to the bare TNS or TNS-HRP and the hydrodynamic radius remained small, around 100 nm. This result again underpins the presence of electrosteric repulsive forces, which predominate over the van der Waals attractions.

The enzymatic assays were performed with TNS-HRP-PDADMAC-SOD-PSS, TNS-HRP and TNS-HRP-PDADMAC-SOD subsystems. The inhibition curve in the SOD assay recorded for the TNS-HRP-PDADMAC-SOD-PSS (Fig. 7a) indicates an improved activity in O_2^- dismutation compared to TNS-PDADMAC-SOD-PSS-HRP. The IC_{50} and the maximum inhibition values measured with the second studied system were 0.38 mg/L and 80%, respectively (Table 1). These values are much closer to the one of the native SOD, therefore highlighting the importance of the localization of SOD in the cascade system. As a result, the activity of SOD has been remarkably improved by locating it in the outer layer of the composite material.

The HRP activity of the TNS-HRP-PDADMAC-SOD-PSS material was also determined (Fig. 7b). The K_m value was found to be 15.50 mM, while the maximum reaction rate was 0.34 mM/s. These values are comparable to the sub-systems (Table 1). More importantly, they indicate lower HRP-like activity than for the native enzyme, but higher than the one measured for TNS-PDADMAC-SOD-PSS-HRP. These findings clearly emphasize the importance of both enzymes (SOD and HRP) location in the multilayered system.

Accordingly, antioxidant dual enzyme systems of remarkable activities were obtained by applying either orders in the sequential adsorption procedure. The functions of both SOD and HRP were maintained during immobilization, however, no evidence was shown for their combined action. This can be further investigated for instance in cellular studies, while reducing ROS-induced oxidative stress.

The above results provide a research direction towards the development of dual enzyme-based antioxidant systems to be applied in industry or biomedical treatments. For instance, titania materials are used to protect skin against sunburn in cosmetics [65], while recovery treatment of UV radiation affected skin is possible with antioxidant enzymes [66] and also with their immobilized forms [67]. Therefore, the present composites containing the dual enzyme system are very promising candidates as additives in skin protecting products. Besides, the future application of the developed hybrid material in treatment of inflammatory bowel diseases is also possible [68]. In these treatments, rectal injection is applied as administering method. However, native antioxidant enzymes lose their activity during the process and thus, their functional stabilization by immobilization offers a solution for this problem.

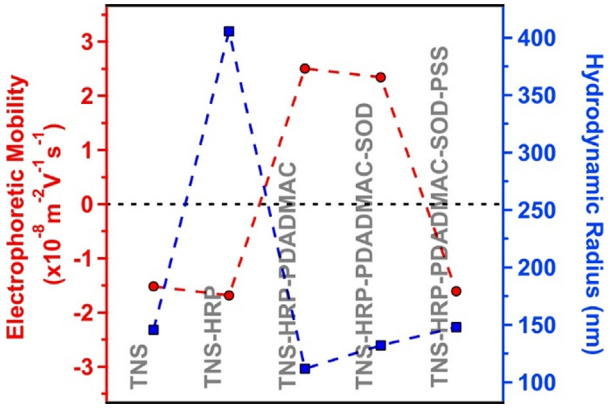

Fig. 8. Electrophoretic mobility (red circle) and hydrodynamic radius (blue square) data during the different steps of the sequential adsorption method. The ionic strength and the TNS concentration were set to 1 mM and 1 mg/L, respectively. The measurement error for both size and mobility is 5%. (For interpretation of the references to colour in this figure legend, the reader is referred to the web version of this article.)

4. Conclusions

In conclusion, SOD and HRP enzymes were successfully co-immobilized on TNS particles using PDADMAC and PSS polyelectrolytes in the sequential adsorption method, in which the order of the components was optimized to achieve the best enzyme activities. The obtained composite possessed high colloidal stability, i.e., excellent resistance against salt-induced aggregation was achieved, and showed remarkable ROS scavenging ability confirmed in dismutation of superoxide radicals and in consumption of hydrogen peroxide. These results shed light on the fact that co-immobilization of antioxidant enzymes is possible on nanoparticulate support without significant loss of the enzymatic activities. Although single SOD and HRP enzymes have already been embedded in composite materials [13,18,20,22], their joint confinement in the present nanostructure gives rise to a wider spectrum for scavenging of ROS including simultaneous decomposition of O_2^- and H_2O_2. Based on these results, the developed cascade systems are potential candidates to reduce the ROS level, i.e., to combat oxidative stress, in liquid medium, where colloidal stability is an important parameter. Potential applications involve cosmetic products for skin protection against sunburn and related treatment of UV radiation damage for skin cells as well as therapy for inflammatory bowel diseases applying rectal injection as administration method.

CRediT authorship contribution statement

Szilárd Sáringer: Investigation, Formal analysis, Visualization, Writing - original draft. **Paul Rouster:** Investigation, Conceptualization. **Istvan Szilagyi:** Conceptualization, Funding acquisition, Writing - review & editing.

Declaration of Competing Interest

The authors declare that they have no known competing financial interests or personal relationships that could have appeared to influence the work reported in this paper.

Acknowledgements

This research was supported by the Lendület program of the Hungarian Academy of Sciences (96130) and by the Ministry of Human Capacities, Hungary through the project 20391-3/2018/FEKUSTRAT. The support from the University of Szeged Open Access Fund (5139) is gratefully acknowledged.

Appendix A. Supplementary material

Supplementary data to this article can be found online at https://doi.org/10.1016/j.jcis.2021.01.012.

References

[1] C.C. Winterbourn, Reconciling the chemistry and biology of reactive oxygen species, Nat. Chem. Biol. 4 (2008) 278–286.
[2] C. Nirmala, M.S. Bisht, H.K. Bajwa, O. Santosh, Bamboo: A rich source of natural antioxidants and its applications in the food and pharmaceutical industry, Trends Food Sci. Technol. 77 (2018) 91–99.
[3] J.W. Finley, A.N. Kong, K.J. Hintze, E.H. Jeffery, L.L. Ji, X.G. Lei, Antioxidants in foods: State of the science important to the food industry, J. Agric. Food Chem. 59 (2011) 6837–6846.
[4] A. Bafana, S. Dutt, S. Kumar, P.S. Ahuja, Superoxide dismutase: an industrial perspective, Crit. Rev. Biotechnol. 31 (2011) 65–76.
[5] L. Wang, Y. Li, L. Zhao, Z. Qi, J. Gou, S. Zhang, J.Z. Zhang, Recent advances in ultrathin two-dimensional materials and biomedical applications for reactive oxygen species generation and scavenging, Nanoscale 12 (2020) 19516–19535.
[6] B.N. Ames, M.K. Shigenaga, T.M. Hagen, Oxidants, antioxidants, and the degenerative diseases of aging, Proc. Natl. Acad. Sci. U. S. A. 90 (1993) 7915–7922.
[7] J. Richardson, K.A. Thomas, B.H. Rubin, D.C. Richardson, Crystal structure of bovine Cu, Zn superoxide dismutase at 3A resolution – Chain tracing and metal ligands, Proc. Natl. Acad. Sci. U. S. A. 72 (1975) 1349–1353.
[8] M. Gajhede, D.J. Schuller, A. Henriksen, A.T. Smith, T.L. Poulos, Crystal structure of horseradish peroxidase C at 2.15 angstrom resolution, Nat. Struct. Biol. 4 (1997) 1032–1038.
[9] H. Sies, Oxidative stress: Oxidants and antioxidants, Exp. Physiol. 82 (1997) 291–295.
[10] R.M. Daniel, M. Dines, H.H. Petach, The denaturation and degradation of stable enzymes at high temperatures, Biochem. J. 317 (1996) 1–11.
[11] D. Constantinescu, H. Weingartner, C. Herrmann, Protein denaturation by ionic liquids and the Hofmeister series: A case study of aqueous solutions of ribonuclease A, Angew. Chem.-Int. Edit. 46 (2007) 8887–8889.
[12] R.A. Sheldon, S. van Pelt, Enzyme immobilisation in biocatalysis: why, what and how, Chem. Soc. Rev. 42 (2013) 6223–6235.
[13] M. Pavlovic, P. Rouster, I. Szilagyi, Synthesis and formulation of functional bionanomaterials with superoxide dismutase activity, Nanoscale 9 (2017) 369–379.
[14] A. Popat, S.B. Hartono, F. Stahr, J. Liu, S.Z. Qiao, G. Qing (Max) Lu, Mesoporous silica nanoparticles for bioadsorption, enzyme immobilisation, and delivery carriers, Nanoscale 3 (2011) 2801, https://doi.org/10.1039/c1nr10224a.
[15] R.C. Rodrigues, C. Ortiz, Á. Berenguer-Murcia, R. Torres, R. Fernández-Lafuente, Modifying enzyme activity and selectivity by immobilization, Chem. Soc. Rev. 42 (2013) 6290–6307.
[16] U. Hanefeld, L.Q. Cao, E. Magner, Enzyme immobilisation: fundamentals and application, Chem. Soc. Rev. 42 (2013) 6211–6212.
[17] B. Katana, P. Rouster, G. Varga, S. Muráth, K. Glinel, A.M. Jonas, I. Szilagyi, Self-assembly of protamine biomacromolecule on halloysite nanotubes for immobilization of superoxide dismutase enzyme, ACS Appl. Bio Mater. 3 (2020) 522–530.
[18] P. Rouster, M. Pavlovic, I. Szilagyi, Immobilization of Superoxide Dismutase on polyelectrolyte functionalized titania nanosheets, ChemBiochem 19 (2018) 404–410.
[19] K. Kamada, A. Yamada, N. Soh, Enhanced catalytic activity of enzymes interacting with nanometric titanate nanosheets, RSC Adv. 5 (2015) 85511–85516.
[20] P. Rouster, M. Pavlovic, S. Sáringer, I. Szilagyi, Functionalized titania nanosheet dispersions of peroxidase activity, J. Phys. Chem. C 122 (2018) 11455–11463.
[21] X. Lang, L. Zhu, Y. Gao, I. Wheeldon, Enhancing enzyme activity and immobilization in nanostructured inorganic-enzyme complexes, Langmuir 33 (2017) 9073–9080.
[22] M. Pavlovic, P. Rouster, Z. Somosi, I. Szilagyi, Horseradish peroxidase-nanoclay hybrid particles of high functional and colloidal stability, J. Colloid Interface Sci. 524 (2018) 114–121.
[23] A. Grotzky, E. Altamura, J. Adamcik, P. Carrara, P. Stano, F. Mavelli, T. Nauser, R. Mezzenga, A.D. Schlüter, P. Walde, Structure and enzymatic properties of molecular dendronized polymer-enzyme conjugates and their entrapment inside giant vesicles, Langmuir 29 (2013) 10831–10840.
[24] A. Grotzky, T. Nauser, H. Erdogan, A.D. Schlüter, P. Walde, A fluorescently labeled dendronized polymer-enzyme conjugate carrying multiple copies of two different types of active enzymes, J. Am. Chem. Soc. 134 (2012) 11392–11395.
[25] A. Niecikowska, M. Krasowska, J. Ralston, K. Malysa, Role of surface charge and hydrophobicity in the three-phase contact formation and wetting film stability under dynamic conditions, J. Phys. Chem. C 116 (2012) 3071–3078.
[26] S. Kment, F. Riboni, S. Pausova, L. Wang, L.Y. Wang, H. Han, Z. Hubicka, J. Krysa, P. Schmuki, R. Zboril, Photoanodes based on TiO_2 and alpha-Fe_2O_3 for solar water splitting - superior role of 1D nanoarchitectures and of combined heterostructures, Chem. Soc. Rev. 46 (2017) 3716–3769.
[27] Á. Veres, J. Ménesi, C. Janáky, G.F. Samu, M.K. Scheyer, Q. Xu, F. Salahioglu, M.V. Garland, I. Dékány, Z. Zhong, New insights into the relationship between structure and photocatalytic properties of TiO_2 catalysts, RSC Adv. 5 (2015) 2421–2428.
[28] R. Kun, M. Balázs, I. Dékány, Photooxidation of organic dye molecules on TiO_2 and zinc-aluminum layered double hydroxide ultrathin multilayers, Colloid Surf. A 265 (2005) 155–162.
[29] L.Z. Wang, T. Sasaki, Titanium oxide nanosheets: Graphene analogues with versatile functionalities, Chem. Rev. 114 (2014) 9455–9486.
[30] D.V. Bavykin, F.C. Walsh, Elongated titanate nanostructures and their applications, Eur. J. Inorg. Chem. 2009 (2009) 977–997.
[31] F.U. Rehman, C. Zhao, H. Jiang, X. Wang, Biomedical applications of nano-titania in theranostics and photodynamic therapy, Biomater. Sci. 4 (2016) 40–54.
[32] K. Kamada, Intense emissions from photoproteins interacting with titanate nanosheets, RSC Adv. 4 (2014) 43052–43056.
[33] L. Zhang, Q. Zhang, J. Li, Layered titanate nanosheets intercalated with myoglobin for direct electrochemistry, Adv. Funct. Mater. 17 (2007) 1958–1965.
[34] G. Decher, J.B. Schlenoff, Multilayer Thin Films, Wiley-VCH, Weinheim, 2002.
[35] P. Rouster, M. Dondelinger, M. Galleni, B. Nysten, A.M. Jonas, K. Glinel, Layer-by-layer assembly of enzyme-loaded halloysite nanotubes for the fabrication of highly active coatings, Colloid Surf. B 178 (2019) 508–514.
[36] R.F. de Oliveira, M.L. de Moraes, O.N. Oliveira, M. Ferreira, Exploiting cascade reactions in bienzyme layer-by-layer films, J. Phys. Chem. C 115 (39) (2011) 19136–19140.
[37] D.G. Ramírez-Wong, C. Bonhomme, S. Demoustier-Champagne, A.M. Jonas, Layer-by-layer assembly of brushes of vertically-standing enzymatic nanotubes, J. Colloid Interface Sci. 514 (2018) 592–598.
[38] P. Rouster, M. Pavlovic, I. Szilagyi, Improving the stability of titania nanosheets by functionalization with polyelectrolytes, RSC Adv. 6 (2016) 97322–97330.
[39] P.N. Pusey, Dynamic light scattering, in: P. Lindner, T. Zemb (Eds.), Neutrons, X-Rays and Light, Elsevier Science B.V., Amsterdam, 2002, pp. 203–220.
[40] G. Trefalt, I. Szilagyi, T. Oncsik, A. Sadeghpour, M. Borkovec, Probing colloidal particle aggregation by light scattering, Chimia 67 (2013) 772–776.
[41] A. Zaccone, H. Wu, M. Lattuada, M. Morbidelli, Correlation between colloidal stability and surfactant adsorption/association phenomena studied by light scattering, J. Phys. Chem. B 112 (2008) 1976–1986.
[42] C. Beauchamp, I. Fridovich, Superoxide dismutase – improved assays and an assay applicable to acrylamide gels, Anal. Biochem. 44 (1971) 276–287.
[43] K. Kamada, T. Nakamura, S. Tsukahara, Photoswitching of enzyme activity of horseradish peroxidase intercalated into semiconducting layers, Chem. Mat. 23 (2011) 2968–2972.
[44] LiHui Zhang, C. Gu, J. Xiong, M. Yang, Y. Guo, Hemin-histamine-montmorillonite clay conjugate as a model biocatalyst to mimic natural peroxidase, Sci. China-Chem. 58 (2015) 731–737.
[45] D.R. Doerge, R.L. Divi, M.I. Churchwell, Identification of the colored guaiacol oxidation product produced by peroxidases, Anal. Biochem. 250 (1997) 10–17.
[46] K.A. Johnson, R.S. Goody, The original Michaelis constant: translation of the 1913 Michaelis-Menten paper, Biochemistry 50 (2011) 8264–8269.
[47] I. Popa, G. Gillies, G. Papastavrou, M. Borkovec, Attractive and repulsive electrostatic forces between positively charged latex particles in the presence of anionic linear polyelectrolytes, J. Phys. Chem. B 114 (2010) 3170–3177.
[48] T.T.M. Ho, K.E. Bremmell, M. Krasowska, S.V. MacWilliams, C.J.E. Richard, D.N. Stringer, D.A. Beattie, In situ ATR FTIR spectroscopic study of the formation and hydration of a fucoidan/chitosan polyelectrolyte multilayer, Langmuir 31 (2015) 11249–11259.
[49] S. Sáringer, P. Rouster, I. Szilágyi, Regulation of the stability of titania nanosheet dispersions with oppositely and like-charged polyelectrolytes, Langmuir 35 (2019) 4986–4994.
[50] Y.K. Leong, Interparticle forces arising from an adsorbed strong polyelectrolyte in colloidal dispersions: charged patch attraction, Colloid Polym. Sci. 277 (1999) 299–305.
[51] S. Muráth, S. Sáringer, Z. Somosi, I. Szilagyi, Effect of ionic compounds of different valences on the stability of titanium oxide colloids, Colloids Interfaces 2 (2018) 32.
[52] F. Iselau, T. Phan Xuan, G. Trefalt, A. Matic, K. Holmberg, R. Bordes, Formation and relaxation kinetics of starch-particle complexes, Soft Matter 12 (2016) 9509–9519.

[53] T. Klačić, A. Sadžak, J. Jukić, T. Preočanin, D. Kovačević, Surface potential study of ceria/poly(sodium 4-styrenesulfonate) aqueous solution interface, Colloid Surf. A-Physicochem. Eng. Asp. 570 (2019) 32–38.
[54] G. Fritz, V. Schädler, N. Willenbacher, N.J. Wagner, Electrosteric stabilization of colloidal dispersions, Langmuir 18 (2002) 6381–6390.
[55] D.F. Evans, H. Wennerstrom, The Colloidal Domain, John Wiley, New York, 1999.
[56] E. Piccinini, S. Alberti, G.S. Longo, T. Berninger, J. Breu, J. Dostalek, O. Azzaroni, W. Knoll, Pushing the boundaries of interfacial sensitivity in graphene FET sensors: Polyelectrolyte multilayers strongly increase the debye screening length, J. Phys. Chem. C 122 (2018) 10181–10188.
[57] O. Löhmann, M. Zerball, R. von Klitzing, Water uptake of polyelectrolyte multilayers including water condensation in voids, Langmuir 34 (2018) 11518–11525.
[58] W. Cheng, C.H. Liu, T.Z. Tong, R. Epsztein, M. Sun, R. Verduzco, J. Ma, M. Elimelech, Selective removal of divalent cations by polyelectrolyte multilayer nanofiltration membrane: Role of polyelectrolyte charge, ion size, and ionic strength, J. Membr. Sci. 559 (2018) 98–106.
[59] Z. Somosi, M. Pavlovic, I. Palinko, I. Szilagyi, Effect of polyelectrolyte mono- and bilayer formation on the colloidal stability of layered double hydroxide nanoparticles, Nanomaterials 8 (2018) 986.
[60] R.A. Ghostine, M.Z. Markarian, J.B. Schlenoff, Asymmetric growth in polyelectrolyte multilayers, J. Am. Chem. Soc. 135 (2013) 7636–7646.
[61] E. Seyrek, J. Hierrezuelo, A. Sadeghpour, I. Szilagyi, M. Borkovec, Molecular mass dependence of adsorbed amount and hydrodynamic thickness of polyelectrolyte layers, Phys. Chem. Chem. Phys. 13 (2011) 12716, https://doi.org/10.1039/c1cp20654k.
[62] A. Fuchs, E. Killmann, Adsorption of polyelectrolytes on colloidal latex particles, electrostatic interactions and stability behaviour, Colloid Polym. Sci. 279 (2001) 53–60.
[63] J. Bannister, W. Bannister, E. WOOD, Bovine erythrocyte cupro-zinc protein 1. Isolation and general characterization, Eur. J. Biochem. 18 (1971) 178–186.
[64] C.B. Lavery, M.C. MacInnis, M.J. MacDonald, J.B. Williams, C.A. Spencer, A.A. Burke, D.J.G. Irwin, G.B. D'Cunha, Purification of peroxidase from horseradish (Armoracia rusticana) roots, J. Agric. Food Chem. 58 (2010) 8471–8476.
[65] M. Morsella, N. d'Alessandro, A.E. Lanterna, J.C. Scaiano, Improving the sunscreen properties of TiO_2 through an understanding of its catalytic properties, ACS Omega 1 (2016) 464–469.
[66] H.R. Rezvani, C. Ged, B. Bouadjar, H. de Verneuil, A. Taïeb, Catalase overexpression reduces UVB-induced apoptosis in a human xeroderma pigmentosum reconstructed epidermis, Cancer Gene Ther. 15 (2008) 241–251.
[67] A.M. Pudlarz, E. Czechowska, M.S. Karbownik, K. Ranoszek-Soliwoda, E. Tomaszewska, G. Celichowski, J. Grobelny, E. Chabielska, A. Gromotowicz-Poplawska, J. Szemraj, The effect of immobilized antioxidant enzymes on the oxidative stress in UV-irradiated rat skin, Nanomedicine 15 (2020) 23–39.
[68] F.A. Moura, K.Q. de Andrade, J.C.F. dos Santos, O.R.P. Araújo, M.O.F. Goulart, Antioxidant therapy for treatment of inflammatory bowel disease: Does it work?, Redox Biol. 6 (2015) 617–639.